

Chemically Modified Tetracyclines as Inhibitors of MMP-2 Matrix Metalloproteinase: A Molecular and Structural Study

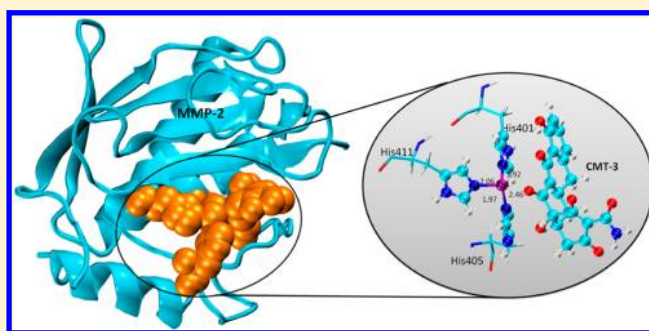
Bruna L. Marcial,^{†,‡} Sergio F. Sousa,^{*,†} Ingrid L. Barbosa,[‡] Helio F. Dos Santos,^{*,‡} and Maria J. Ramos[†]

[†]REQUIMTE, Departamento de Química e Bioquímica, Faculdade de Ciências, Universidade do Porto, Rua do Campo Alegre, s/n, 4169-007, Porto, Portugal

[‡]Núcleo de Estudos em Química Computacional (NEQC), Departamento de Química – ICE, Universidade Federal de Juiz de Fora, Juiz de Fora, MG, 36036-330, Brazil

S Supporting Information

ABSTRACT: The present study focuses on the direct interaction of chemically modified tetracyclines (CMTs) with the active site of the matrix metalloproteinase 2 (MMP-2). Molecular docking, molecular dynamics (MD) simulations, and free energy calculations were accomplished for seven CMT derivatives. New sets of parameters are proposed for structural and catalytic zinc atoms in order to study MMPs and their complexes by means of the AMBER force field. Our computational results show that six CMTs studied bind to the catalytic zinc of the MMP-2 enzyme at the O11–O12 site as proposed experimentally. The exception was the CMT-3 analogue that is found embedding within the active site, enhancing the van der Waals and hydrophobic contacts with the hydrophobic S1' pocket in the MMP-2 enzyme. The binding energy calculated in solution predicts the CMT-3 complexes as the most favorable, followed by the CMT-7 and CMT-8 analogues, respectively, which is in line with experimental findings. This work is the first step toward understanding the mechanism of CMTs as MMP inhibitors at a molecular level.



■ INTRODUCTION

Matrix metalloproteinases (MMPs) are the family of calcium- and zinc-dependent endopeptidases, which degrade most components of the extracellular matrix (ECM). The MMPs play a key role in tumor invasion, metastasis, and angiogenesis, especially the gelatinases, MMP-2 and MMP-9, which degrade basement membrane type IV collagen and appear essential for cellular invasion.¹ The inhibition of MMP activity is an interesting therapeutic strategy for the treatment of diseases such as cancer. In recent years, a number of MMP inhibitors (MMPis) have been developed. The most studied synthetic MMP inhibitors belong to the hydroxamate family, which covalently bind to the zinc atom at the MMP active site.² As an alternative, tetracycline (TC) derivatives have currently been considered as potential MMP inhibitors, showing promising results in preclinical cancer models. However, their exact action mechanism has not been completely understood yet.³ The TC derivatives constitute a family of molecules with broad-spectrum antimicrobial activity. In addition to their antimicrobial properties, some new analogues, named chemically modified tetracycline (CMTs) (see Figure 1), which in general lack the dimethylamino (DMA) group at the C4,⁴ have been tested as MMP inhibitors. The main advantage of CMTs over the parent TC is that the former do not result in resistant microorganisms, which is a common side-effect of antibiotic therapy.^{5,6}

The goal of this study is to get molecular insights on the interaction of CMTs with the catalytic site of MMPs. The catalytic zinc ion, located in the active site of MMPs, is the target of different compounds called zinc binding groups (ZBGs), designed to block the active site and the enzymatic activity. The CMT derivatives (Figure 1) have proved to be effective as MMP inhibitors *in vitro* and *in vivo*.^{3,7} Particularly, the CMT-3 analogue (also known as COL-3) has been found to inhibit cancer cell invasion and metastasis. In a phase-II study, COL-3, when administered at 50 mg/day, demonstrated antitumor activity, resulting in significant decline of MMP-2 and MMP-9 plasma levels.⁸ Among possible mechanisms of action for CMTs discussed recently in a special issue of *Pharmacol. Res.*,^{5,6,9} the CMT chelation with metal ions plays a major role in the MMP inhibition. The data obtained *in vitro* applying a spectrophotometric technique suggested that the CMT-*n* coordination with Zn is positively related to the potency of these compounds.¹⁰ Therefore, the inhibitory potential of CMTs might be affected by structural differences among their derivatives.

In a recent study, using simple molecular models for the zinc-active site of MMP, we demonstrated that the structures of the

Received: August 10, 2012

Revised: October 27, 2012

Published: November 1, 2012

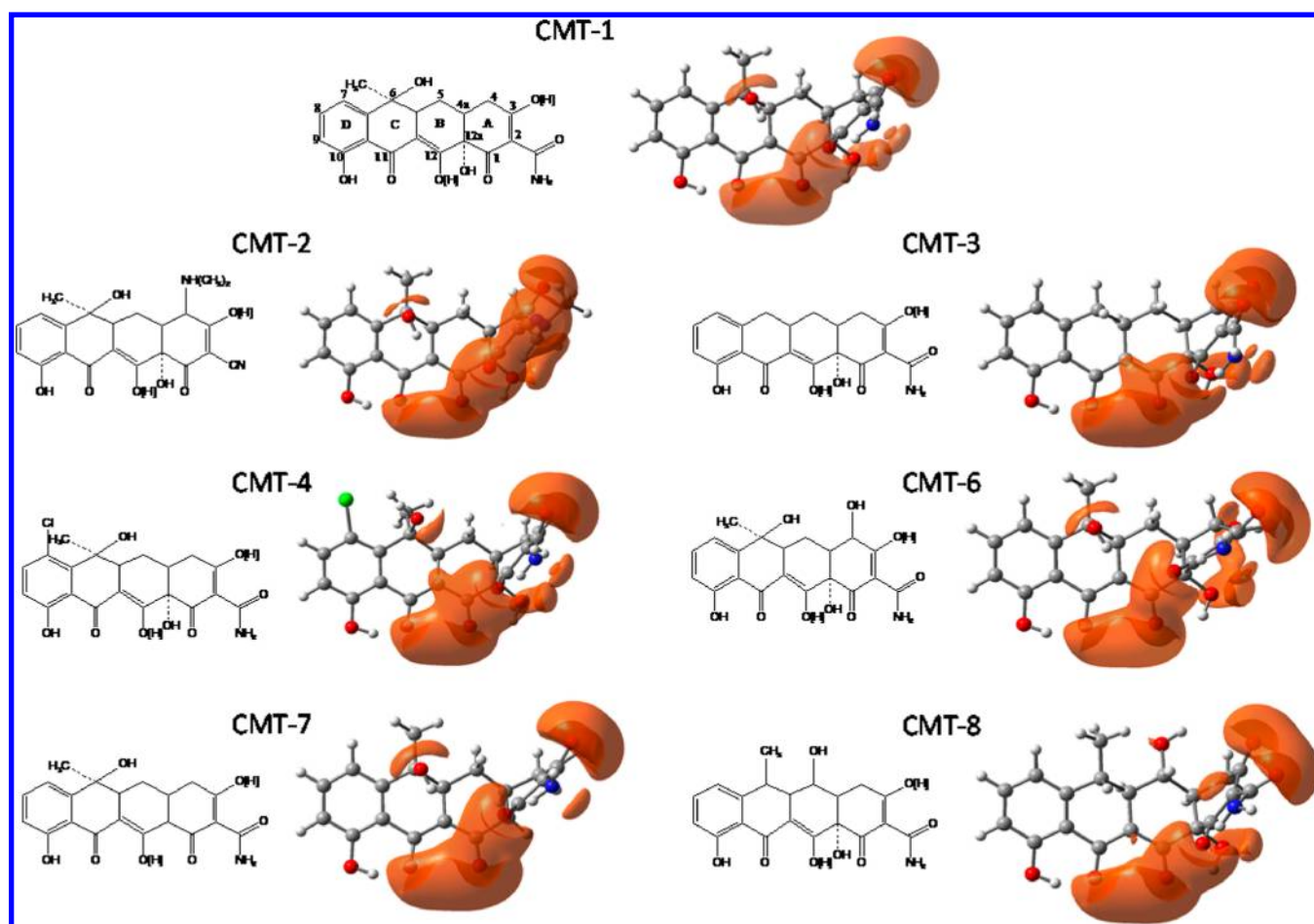


Figure 1. Structures of chemically modified tetracyclines and the molecular electrostatic potentials (MEPs) generated at the B3LYP/6-31G(d) level.

CMTs interfere significantly with the coordination mode to the Zn(II) ion.¹¹ Herein, a more systematic evaluation of the relationship between the molecular properties of CMTs and their interactions with the catalytic Zn ion in MMP-2 was conducted using a combined docking and molecular dynamics (MD) simulation. These analyses were further complemented with an energetic evaluation of the resulting binding conformations with the molecular mechanics/Poisson–Boltzmann surface area (MM-PBSA) and thermodynamic integration (TI) methods. The results discussed here might assist in structure-based design of MMP inhibitors based on TC structure with improved biological response.

THEORETICAL CALCULATIONS

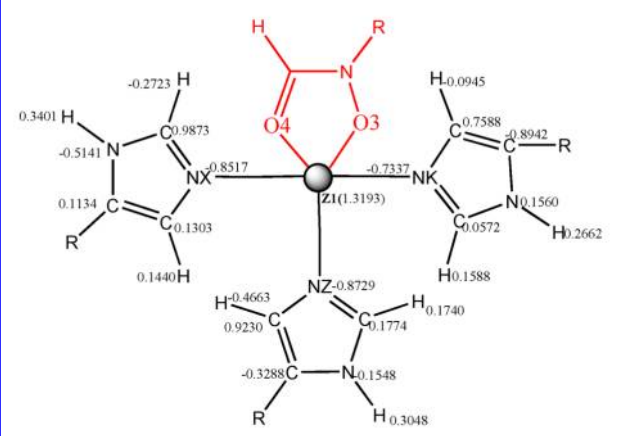
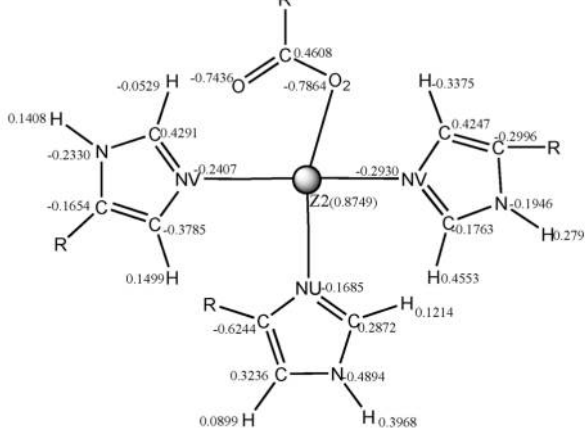
Molecular Docking. The X-ray structure of gelatinase A catalytic domain complexed with a hydroxamate inhibitor determined by Dhanaraj et al. (PDB file 1QIB) with 2.8 Å of resolution was obtained from the Protein Data Bank.¹² The water molecules were extracted and the hydrogen atoms added to the enzyme by setting the pH to 7.0.

The CMT-*n* ligands' structures, in which *n* means 1, 2, 3, 4, 6, 7, and 8 (Figure 1), were optimized at the B3LYP/6-31G(d)^{13–16} level using Gaussian 09.¹⁷ The molecular electrostatic potentials for the optimized geometries have been generated using the CUBEGEN utility available in the Gaussian 09 package. The molecular electrostatic potential was mapped onto the 0.2 e/bohr³ electron density surface with Gaussianview 5.0.

The ligands were docked onto the active site of MMP-2 using AutoDock 4.0.¹⁸ The docking files were prepared with the Vslab package.¹⁹ The partial atomic charges for the ligands were obtained at the B3LYP/6-31G(d) level. The nonbonded zinc parameters used were as follows: radius = 1.1 Å, well depth = 0.25 kcal/mol, charge = +2.0e.²⁰ The grid size was set to 80 × 80 × 80 points with a grid spacing of 0.275 Å centered on the zinc ion in the crystal structure (1QIB).¹² The docking simulations were performed using the Lamarckian genetic algorithm (LGA) with 100 solutions for each ligand obtained. The best poses were based on two criteria, the distance of the CMT-*n* groups from the catalytic zinc ion and the autodock scoring function. It is important to notice that the 3D structure of the MMP-2 enzyme used in this study presents the catalytic domain complexed with a hydroxamate inhibitor (1QIB),¹² but the inhibitors' coordinates were not deposited at the PDB; thus, our protocol was first successfully tested for the MMP-9 complexed with reverse hydroxamate inhibitor (PDB file 1GKC);²¹ the conformation and the main hydrogen interactions resulting from molecular docking calculations were in good agreement with the experimental structural data, validating the protocol chosen (see Figure S1, Supporting Information).

Minimization and MD Simulations. To provide refined analyses of the molecular interactions between the CMTs and the active site of MMP-2, MD simulations were performed for the seven MMP-2:CMT-*n* complexes obtained as the best solution from molecular docking calculations.

Table 1. Parameters Calculated for the Structural and Catalytic Zinc Binding Sites^a

Catalytic zinc binding site			Structural zinc binding site		
					
Bonds	R_{eq} (Å)	K_r (kcal mol ⁻¹ Å ⁻²)	Bonds	R_{eq} (Å)	K_r (kcal mol ⁻¹ Å ⁻²)
Z1-NX	2.09	66.4	Z2-O2	1.98	72.2
Z1-NK	2.09	66.4	Z2-NV	2.05	78.9
Z1-NZ	2.20	37.0	Z2-NU	2.09	59.3
Angles	θ (°)	K_θ (kcal mol ⁻¹ rad ⁻²)	Angles	θ (°)	K_θ (kcal mol ⁻¹ rad ⁻²)
NX-Z1-NK	113.1	15.6	NV-Z2-NU	107.7	15.2
NX-Z1-NZ	96.33	33.0	NV-Z2-NV	116.3	13.5
NK-Z1-NZ	96.33	33.0	O2-Z2-NU	96.9	32.4
			O2-Z2-NV	113.1	17.9

^aThe atomic charges are represented inset the structure representation (in au).

There are several works in the literature addressing the theoretical description of metal ions in metalloenzymes. Aqvist and Warshel applied the cationic dummy atoms to represent metal ions in different metalloenzymes.²² This method was extensively tested and proved to be reliable to describe the solvation free energy and structures of small models containing transition metals such as octahedrally coordinated bivalent manganese ions in solution,²³ tetrahedrally bivalent zinc ion in human carbonic anhydrase I and carboxypeptidases A^{24,25} and binuclear zinc ion in bacterial metallo- β -lactamases IMP-1 and IMP-6²⁶ as well as octahedrally coordinated bivalent earth alkali magnesium ion in the binuclear active site of DNA polymerases.²⁷ The major limitation in this approach is the lack of covalent bond or constraints in the metal coordination sphere. As alternatives, two main approaches have been used to model the force field for the metal ions: (1) the nonbonded method, in which van der Waals and nonbonded electrostatic terms are used to model the metal–ligand interaction, and (2) the bonded method where the interactions between the metal and ligand/enzyme are described by the bonded terms, including bond stretching.^{20,28–32} Regarding the zinc–metal proteins, both of the models have been used. Donini and Kollman carried out MM-PBSA and MM-GBSA calculations on certain ligands complexed with different MMPs using the zinc nonbonded model.³⁰ Zhang et al. reported the MD and free energy perturbation to study enzyme–inhibitor complexes of MMP-2-hydroxamate using the zinc-bonded model.³² In the present work, we used the bonded model for structural zinc by explicitly bonding the Zn2 ion with the HIS190-N ϵ , HIS175-N ϵ , HIS203-N δ , and ASP177-O δ atoms; for the catalytic zinc, we employed the hybrid bonded/nonbonded approach in which the Zn1 ion is linked to the HIS226-N ϵ , HIS230-N ϵ , and HIS236-N ϵ atoms, whereas metal–inhibitor binding is represented through the nonbonded approach. We claim that

this description is very reasonable, because it can represent in detail the metal/enzyme interactions while ensuring at the same time inhibitor binding flexibility. In order to improve the force field, we have explicitly parametrized the bond, angles, and charges associated with the zinc ion and its interaction with the MMP. For the calcium ion, we used the nonbonded representation proposed by Aqvist.³³ The parameters calculated for the structural zinc and the catalytic zinc complexed with hydroxamate inhibitors by quantum mechanical methods were subsequently tested. After the validation, these parameters were used for MD simulations for the MMP–inhibitor system.

Force Field. Two distinct molecular zinc models for the catalytic (Z1) and structural (Z2) zincs in the MMP were built from the crystallographic structure of the MMP-9 complexed with reverse hydroxamate (PDB file 1GKC).²¹ The simplest modeling of the amino acid side chains and hydroxamate functional group were used as shown in Table 1. The potential energy curves were calculated through routine scans for bond stretching and angle bending, starting from the fully optimized geometry of the model using the hybrid B3LYP functional and 6-31G(d) basis set for ligand atoms. For Zn, the Stuttgart/Dresden effective core potentials (ECPs) and the corresponding SDD valence basis set (8s6p3d valence basis set for Zn)³⁴ were used. For the catalytic zinc (Z1), the semirigid scan was performed keeping the hydroxamate functional group frozen, because we were interested in calculating the parameters for the zinc/MMP interaction. The force constants for the bonds (K_r) and angles (K_θ) involving the zinc center were obtained by fitting a second-order polynomial function to the reference data. The final set of parameter values is listed in Table 1. For the angles in which Zn was a terminal atom, parameters were obtained from other Zn enzymes in the literature.³⁵ All the dihedral parameters involving the Zn–ligand interactions were set to zero.^{36,37} This approximation has been used with success

in the study of several different metalloenzymes.^{32,37,38} All quantum mechanics calculations were done using Gaussian 09.¹⁷

Partial Charges. We first developed an appropriate electrostatic representation of the MMP active and structural sites. Restrained electrostatic potential fit (RESP)^{39,40} charges were derived at the B3LYP/6-311++G(3df,2pd) level for the zinc ions and their chemical surroundings. The models were built for the same crystallographic structure used in the force constant calculation (see Table 1) but including the zinc ion and the full amino acid residues in its coordination sphere (these molecular models were also optimized at the B3LYP/SDD/6-31G(d) level). For the hydroxamate inhibitor, RESP charges were derived at the HF/6-31G(d) level and the force-field parameters were taken from the general AMBER force field (GAFF),⁴¹ which is specialized for small organic molecules.

Table 1 shows the partial charges derived for the three histidines coordinated to the catalytic zinc, the three histidines and one aspartate coordinated to structural zinc ion, in addition to the partial charge for the two zinc ions. The atom types were defined in conformity with the AMBER force field^{42–44} with some modifications to the AMBER database and PDB files. For the structural zinc (Z2), we defined the new residues HI1, HI2, HI3, and AS1 representing HIS190, HIS203, HIS175, and ASP177, respectively. For the catalytic zinc (Z1), we defined the new residues HIA, HIB, and HIC representing HIS401, HIS405, and HIS411, respectively (the residue numbers are in accordance with the 1GKC structure). Finally, we created the new AMBER library files describing these two metal coordination spheres, which are available as Supporting Information.

Parameter Validation. To test the parameters obtained and to verify whether they could be used for our MD simulations, we carried out 12 ns MD on the X-ray structure of MMP-9 (1GKC) complexed with the reverse hydroxamate inhibitors using our set of modified parameters given in Table 1. The systems were surrounded by a periodic box of TIP3P water molecules, with a minimum distance of 12 Å between the enzyme and the box side. Sodium ions were placed using the Leap program to neutralize the negative charges of the solution. Before carrying out MD simulations, four steps of minimizations were performed using the SANDER module of AMBER 10.⁴⁵ In the first step, we kept the protein fixed with a constraint of 50 kcal mol^{−1} and only the positions of the water molecules were minimized; then, in the second step, these constraints were applied only to the heavy atoms, and the third step was limited to the backbone α carbon (CA). The last step was a full energy minimization without constraint force.

MD trajectories were run using the minimized structure as a starting input in the PMEMD program included in the AMBER 10 package⁴⁵ and considering periodic boundary conditions to simulate a continuous system. The SHAKE algorithm⁴⁶ was employed to keep all bonds involving hydrogen atoms rigid, and the time step of the simulations was 2.0 fs. The particle-mesh Ewald (PME) method was used to include the long-range interactions, and a cutoff of 10 Å for the nonbonded interactions was considered. A 50 ps equilibration procedure followed by 12 ns of constant-pressure MD simulation was carried out at 300 K. To check the validity of parameters^{37,47} developed, the MD trajectory and all structural parameters were analyzed and compared to the set of X-ray structures of MMP enzymes as well as to small models of the active site of MMP

calculated with the quantum chemistry method. It should bear in mind that a more general validation protocol must involve energies as reference properties, as carefully addressed recently by Warshel and co-workers.²⁷ In the present study, only structural parameters are used to validate the new set of parameters and the results are given as Supporting Information (Figures S2–S5). In general, the average RMSD for the backbone C α atoms (CA) and the zinc coordination sphere atoms (Zn core) suggests that the geometries of the two Zn coordination spheres were maintained throughout the entire simulation time (Figure S2, Supporting Information); the same behavior was observed for the bond lengths and angles parametrized for the structural and catalytic zinc coordination spheres in MMP (see Figure S3, Supporting Information). The approach of mixing bonded and nonbonded regions used for the catalytic zinc ion (Z1) appears to be satisfactory to represent the coordination sphere of Zn. Figure S4 (Supporting Information) shows the structure of 1GKC after 12 ns of simulation using the optimized parameters. The distance between the inhibitor and the zinc ion are in agreement with experiment, as shown in Figure S5 (Supporting Information) for several X-ray structures and *ab initio* data. All analyses proved that the new set of parameters is reliable and can be used for further studies involving the series of MMP-2:CMT-*n* complexes.

For the study of the MMP-2:CMT-*n* complexes, we employed the same MD protocol previously tested and validated. We used the FF99 AMBER force field modified with our set of parameters for the metal ion moiety and the CMT-*n*. RESP charges were derived at the HF/6-31G(d) level with the other parameters according to the general Amber force field (GAFF). MD simulations of 12 ns were performed for each system, representing a total of 84 ns of simulation time. The last 6 ns of each simulation were used to calculate the stability of the MMP-2:CMT-*n* complexes.

Calculation of the Binding Free Energy of the Complexes. In order to discuss the relative stability of the MMP-2:CMT-*n* complexes, we have calculated the relative binding free energy ($\Delta\Delta G_{\text{bind}}$) for all the systems. Values for $\Delta\Delta G_{\text{bind}}$ have been calculated with the rigorous thermodynamic integration (TI)^{47,48} method as well as using the faster molecular mechanics/Poisson–Boltzmann surface area (MM-PBSA) methodology.^{49,50} In fact, both of the approaches are indicated to predict the free energy for protein–ligand interactions. The MM-PBSA approach calculates the binding free energy based on the analysis of the conformational ensemble obtained from MD simulation using the continuum model for solvent. Moreover, the MM-PBSA method restricts the simulations to the states before and after binding without including any intermediate states, as done in the TI formalism.⁴⁷ On the other hand, the MM-PBSA approach has the advantages of accounting for large structural changes and affordable computer time.^{49–51} In the present study, the TI method was applied only for two CMT analogues, namely, CMT-3 and CMT-8, which are the main representatives regarding biological effects and for which experimental binding energies are available.⁵² For the other derivatives, the MM-PBSA approach was applied.

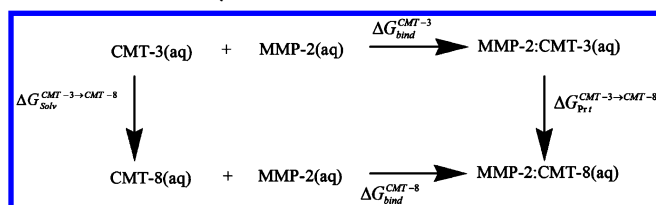
Thermodynamic Integration. TI is one of the most rigorous methods to compute relative free energies and was used here to predict the difference in binding free energies for CMT-3 and CMT-8 compounds. In TI calculation, two states A and B are considered to be connected *via* an additional *non-physical*

coordinate, called λ , and a transition from system A to B along this *non*-physical reaction coordination is simulated. The free energy difference between the states can be obtained directly from the configuration integral:

$$\Delta G_{A \rightarrow B}^{\text{TI}} = \int_0^1 \left\langle \frac{\partial V(\lambda)}{\partial \lambda} \right\rangle_{\lambda} d\lambda \quad (1)$$

The difference in Gibbs free energy between the CMT-3 model and the CMT-8 model was evaluated using the thermodynamic cycle shown in Scheme 1.

Scheme 1. Thermodynamic Cycle to Calculate the Free Energy Difference between the CMT-3 and CMT-8 Bound to the MMP-2 Enzyme^a



^a $\Delta G_{\text{bind}}^{\text{CMT-3}}$ and $\Delta G_{\text{bind}}^{\text{CMT-8}}$ are binding free energies for the CMT-3 and CMT-8 ligands, respectively. $\Delta G_{\text{solv}}^{\text{CMT-3} \rightarrow \text{CMT-8}}$ and $\Delta G_{\text{prf}}^{\text{CMT-3} \rightarrow \text{CMT-8}}$ are the nonphysical transformation free energies from CMT-3 to CMT-8 in solution and bound to the MMP-2 enzyme, respectively.

Equation 2 results from the thermodynamic cycle in Scheme 1:

$$\begin{aligned} \Delta \Delta G_{\text{bind}}^{\text{CMT-3} \rightarrow \text{CMT-8}} &= \Delta G_{\text{bind}}^{\text{CMT-8}} - \Delta G_{\text{bind}}^{\text{CMT-3}} \\ &= \Delta G_{\text{prf}}^{\text{CMT-3} \rightarrow \text{CMT-8}} - \Delta G_{\text{solv}}^{\text{CMT-3} \rightarrow \text{CMT-8}} \end{aligned} \quad (2)$$

where the quantities $\Delta G_{\text{prf}}^{\text{CMT-3} \rightarrow \text{CMT-8}}$ and $\Delta G_{\text{solv}}^{\text{CMT-3} \rightarrow \text{CMT-8}}$ must be calculated. These individual values have no meaning in the real world, as they refer to free energy differences between distinct molecules. However, the difference between them, i.e., the difference in the free energy of binding between the CMT-3 and the CMT-8 complexes, is a meaningful value.

In this work, we have considered three separate energy transformations: a first one in which the charges of the atoms that will disappear are removed (ΔG^1); a second one in which atomic species are exchanged with no charges, hence resulting in the calculation of the contribution of the vdW interactions to the free energy difference (ΔG^2); finally, a third one in which the charges of the nascent atoms are switched on and gradually increase (ΔG^3).

$$\begin{aligned} \Delta \Delta G_{\text{bind}}^{\text{CMT-3} \rightarrow \text{CMT-8}} &= \Delta G_{\text{prf}}^{\text{CMT-3} \rightarrow \text{CMT-8}} - \Delta G_{\text{solv}}^{\text{CMT-3} \rightarrow \text{CMT-8}} \\ &= (\Delta G_{\text{prf}}^1 + \Delta G_{\text{prf}}^2 + \Delta G_{\text{prf}}^3) - (\Delta G_{\text{solv}}^1 + \Delta G_{\text{solv}}^2 \\ &\quad + \Delta G_{\text{solv}}^3) \end{aligned} \quad (3)$$

We have computed the free energy by using the thermodynamic integration tools of the SANDER routine implemented in the AMBER 10 package, with modified vdW interactions (soft-core potentials) to ensure smooth free energy curves.⁵³ These simulations were performed in explicit solvent and under periodic boundary conditions for nine λ values (0.1, 0.2, 0.3, 0.4, 0.5, 0.6, 0.7, 0.8, 0.9). For each λ value running in

each transformation, we have carried out a minimization, a constant volume and pressure equilibration, and then a constant pressure production run. Free energy contributions were collected independently for each λ from the production run.

During the λ path, *soft-core* potentials were used following the second energy transformation for nonbonded interaction.⁵⁴ We have used a 9 Å cutoff for the Coulombic interactions, within a particle-mesh Ewald methodology. We used the FF99 AMBER force field modified with our set of parameters for the surrounding metal ions. RESP charges were derived at the HF/6-31G(d) level with the other parameters according to the general Amber force field (GAFF). Conventional protonation states for all amino acids at pH 7 were considered. All the hydrogen atoms were added, and the Na⁺ were placed using the Leap program to neutralize the negative charges of the solution. The systems were surrounded by a periodic box of TIP3P water molecules, with a minimum distance of 12 Å between the enzyme and the box side. The time step used for integrating the equations of motion was 0.001 ps. A total of 50 ps was simulated for constant volume and constant pressure equilibration, and a total of 100 ps for production at 300 K temperature for each λ value. The ensemble average of $\partial V(\lambda)/\partial \lambda$ for each λ point was calculated over the production run. In addition, the hysteresis in the free energy was also evaluated by performing the mutations forward and backward. The total simulation time to mutate the CMT-3 into the CMT-8 was 7.8 ns, and as we performed this in both free and bound states as well as in direct and reverse directions, the total simulation time was 15.6 ns for free and bound species.

Molecular Mechanics/Poisson–Boltzmann Surface Area. The representative snapshots collected along the molecular dynamics trajectories have been treated employing the molecular mechanics/Poisson–Boltzmann surface area (MM-PBSA) methodology⁴⁹ to calculate the binding free energy of a protein–ligand complex in aqueous solution.

According to this methodology, the free energy of binding is described by the following equation:

$$\Delta G_{\text{bind}} = \Delta E_{\text{MM}} + \Delta G_{\text{PB}} + \Delta G_{\text{nonpolar}} \quad (4)$$

The right-hand terms ($\Delta G_{\text{PB}} + \Delta G_{\text{nonpolar}}$) in eq 4 are the contribution of the solvation free energies (ΔG_{solv}), in which the ΔG_{PB} is the difference in the electrostatic contribution to the solvation free energy upon ligand binding, estimated by the resolution of the Poisson–Boltzmann (PB) equation, and $\Delta G_{\text{nonpolar}}$ is the difference in the nonpolar or hydrophobic contribution to the solvation energy upon ligand binding, estimated from the differences in the solvent-accessible surface areas of the protein and ligands, alone and complexed. The ΔE_{MM} is the MM energy of the molecule, obtained by the sum of the internal energy of the molecules (i.e., bonded terms, E_{int}), the electrostatics (E_{ele}), and the van der Waals interactions (E_{vdw}) of representative snapshots from a molecular dynamics (MD) trajectory.

All terms in eq 4 are averages obtained from a number of snapshots taken from MD simulations in bulk explicit solvent and were obtained by the pbsa program, included in the AMBER 10 package. In our calculations, one snapshot was extracted at each 20 ps of simulation, resulting in a total of the 300 snapshots that were used for the energy calculations for each ligand and thus a total of 2100 energy calculations were carried out with the sander module of Amber. The entropy contribution to the free energy was not calculated. Considering

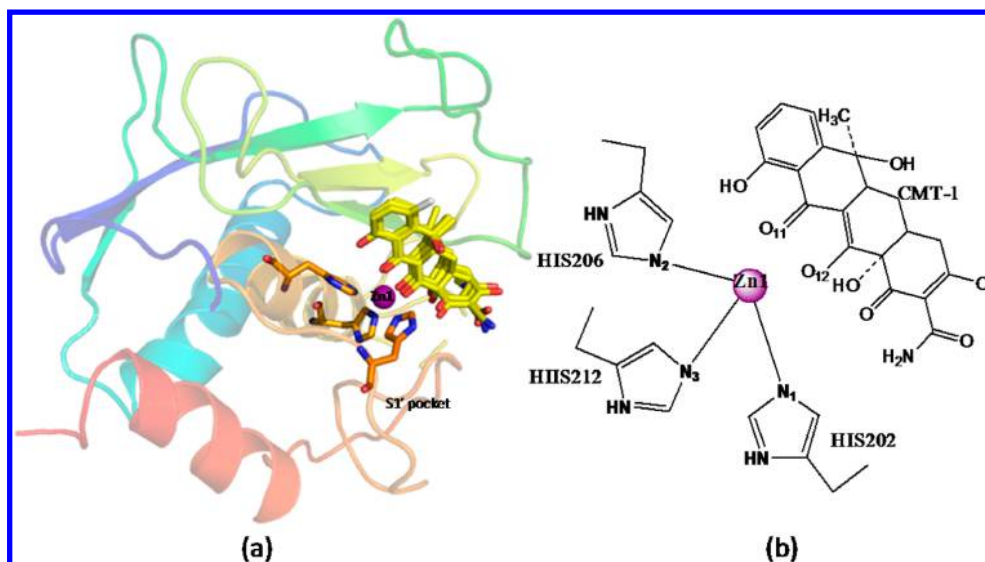


Figure 2. (a) Structures of some CMT-*n* docked in the MMP-2. (b) The CMT-1 coordination scheme (the residue number is in accord with the 1QJB structure).

the similarity between the CMT-*n* ligands, we assumed that the entropic contributions to the $\Delta\Delta G_{\text{bind}}$ cancel out and are negligible.

In this work, the MM-PBSA results were in satisfactory agreement with TI values for the CMT-3 \rightarrow CMT-8 process, supporting our protocol with external and internal dielectric constants set to 80.0 and 4.00, respectively. A similar protocol was described recently by one of us to predict the substrate recognition in HIV-1 protease and showing very accurate results.⁵⁵

RESULTS AND DISCUSSION

To explore and clarify the possible action mechanism of the CMT-*n* derivative as inhibitors of MMPs (i.e., the CMT coordinating with the catalytic zinc of the enzyme), we have modeled the complex of the MMP-2 enzyme with some CMT-*n* molecules. The chemically modified tetracyclines used were the CMT-1, CMT-2, CMT-3, CMT-4, CMT-6, CMT-7, and CMT-8 (see Figure 1); these are the non-antimicrobial tetracyclines and have presented potential activity as MMP inhibitors.^{3,6}

Ligand. The optimized geometries of the ligands obtained at the B3LYP/6-31G(d) level as well as their negative potential isosurfaces are shown in Figure 1. It can be observed that all the CMTs present common patterns in the electrostatic potential surface. In fact, the most negative potential is located in the oxygen atoms of carbonyl groups C3–C2 at ring A of CMT and the β -diketone moieties at C11 and C12 at ring B–C of CMT. These regions represent the possible hydrogen bond receptors, which will stabilize the ligands in the complex with the catalytic domain. Interestingly, the region of ring A is the only part of the TC derivative framework that is known to adopt several alternative conformations. This is verified by quantum mechanical and molecular mechanical calculations for tetracycline and analogues in the so-called extended and twisted conformations of the zwitterionic tautomer.^{56–60} The region of the rings B–C–D is a common coordination site in tetracycline for alkaline and alkaline earth metals. The binding of proteins, including TetR, involves the TC coordination with bivalent metal ions such Ca(II) and Mg(II) at the O11–O12 site. This

is also the main binding site of CMT with zinc ion in MMPs. This is supported by the study of the analogue CMT-5, a pyrazole derivative, which does not present MMP-inhibitory activity *in vitro*.⁶¹ For CMT-5, the β -diketone moieties at C11 and C12 were replaced by nitrogen atoms, eliminating the most important Ca(II)- and Zn(II)-binding site. In our previous paper,¹¹ we also showed that coordination at O11–O12 is preferred for the most active CMTs, namely, CMT-3 and CMT-8.

Docking. The first step to explore the MMP:CMT-*n* interaction was to apply the docking procedure to construct the starting structures of the complexes. The CMT-*n* molecules were docked into the active site of MMP-2 (PDB file 1QJB),¹² and the best ranking of poses was analyzed. Except for CMT-3, all others CMT-*n*'s showed similar arrangement in the binding site (see Figure 2). They present the O11–O12 site of CMT-*n* close to the zinc ion; the average distances from catalytic zinc ion to the hydroxyl (O11) and carbonyl (O12) oxygens for the selected complexes were 2.01 ± 0.17 and 1.91 ± 0.11 Å, respectively. These values suggest that the CMT-*n* is in the coordination sphere of the metal, as observed experimentally for the hydroxamate complexes.⁶²

The CMT-3 analogue appears inside the S1' subsite, also named the selectivity pocket, which is described as a tunnel leading toward the solvent in the gelatinase structures and represents the main difference between the catalytic domain of the various MMPs.⁶³ This result could be explained by the structural differences in the CMTs. The CMT-3 molecule is the simplest tetracycline derivative, without bulky substituents at the C4, C6, and C7 positions (see Figure 1). This suggests that the steric hindrance, due to the bulky groups at position C6, determines how the CMTs interact with the MMP-2 target and play a major role in the protein–ligand binding. Interestingly, the most potent MMP inhibitors have been designed on the basis of the hydroxamic acid ZBG with substituents that provide the occupation of the S1' and S2' enzymes' subsites.⁶³ The majority of the CMT analogues have substituents at the C6 position, which might explain the higher specificity and biological potency of the CMT-3 molecule.

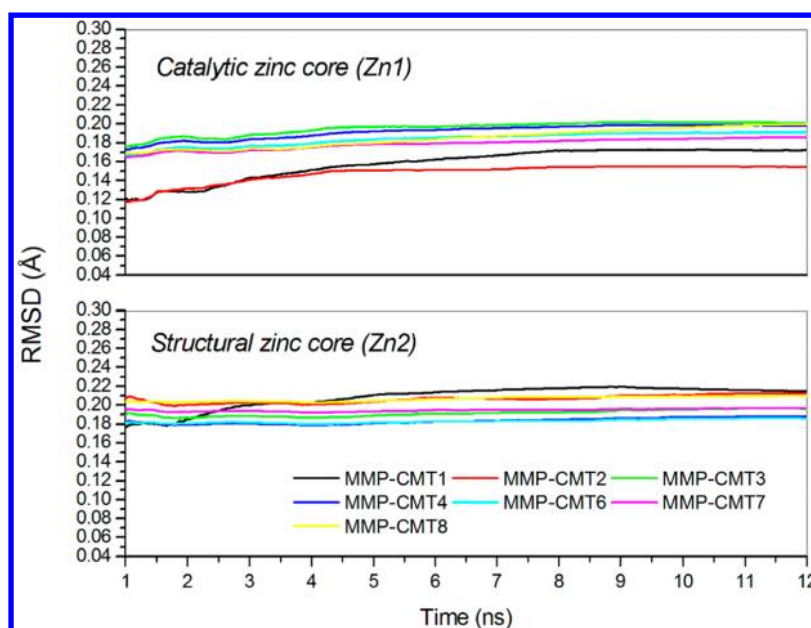


Figure 3. Plot of the cumulative root-mean-square deviation (RMSD) variations in the MD simulations performed for MMP-2:CMT-*n*. The Zn core RMSD refers to the atoms in the Zn coordination sphere.

Molecular Dynamics and Relative Stability Analysis of CMT-*n* Complexes. The seven docked structures of MMP-2-CMT-*n* complexes were subjected to MD simulations using the bonded approach for the zinc ion and the atoms of the enzyme, and the nonbonded approach to the CMT-*n* coordinated with catalytic zinc. This model was used to give more flexibility to the ligand, allowing inhibitor decoordination or readjustment. The MD protocol used was previously tested for the MMP-9-reverse hydroxamate complex, for which a minimized structure (more details in the Supporting Information) in complete agreement with the X-ray structure²¹ was obtained.

Figure 3 shows the cumulative average of root-mean-square deviation (RMSD) variation in the MD simulations for the amino acid atoms in the zinc coordination sphere (the Zn1 and Zn2 cores were defined in analogy with the models described in Figure 2). We can observe that the values are notably constant, which suggests that the geometries of the structural and catalytic Zn coordination spheres are maintained during the course of the simulation time for all CMT-*n* tested in this work.

Table 2 presents some structural parameters calculated for the seven MMP-2:CMT-*n* compounds. In the crystallographic structure (PDB file 1QIB), the Zn is coordinated to the nitrogens of three histidines: HIS202 (N1), HIS206 (N2), and HIS212 (N3) with Zn–N bond lengths of 2.31, 2.33, and 2.36 Å, respectively. After MD simulations for the MMP-2:CMT-*n* complexes, the calculated Zn–N bond lengths range from 1.86 to 2.26 Å (see Table S2, Supporting Information). These differences in the bond distance are due to the change of the environment of the zinc coordination sphere, and also a consequence of the interaction with the CMT-*n* ligand. The average bond distances of the Zn–O11 and Zn–O12 from the CMT-*n* ligand were 2.5 ± 0.3 and 2.3 ± 0.1 Å, respectively. The larger values of these parameters were found for the CMT-3 complex, for which the Zn–O11 distance was around 3.4 Å. This weak interaction is due to the different position of the CMT-3 inside the active site and the interaction with the hydrophobic region of the S1' pocket of MMP-2 enzyme. The other CMT-*n* ligands present Zn–ligand distances comparable

Table 2. Structural Data for MMP-2-CMT-*n* Complexes Obtained from MD Simulation

ligand	bond length (Å)		angle (deg)			τ
	O11–Zn	O12–Zn	O12–Zn–N2	O11–Zn–N1	N2–Zn–N3	
CMT-1	2.42	2.39	165.44	166.76	92.17	0.02
CMT-2	2.53	2.32	175.08	160.62	84.04	0.07
CMT-3	3.40	2.46	155.58	70.73	88.25	
CMT-4	2.37	2.40	152.22	160.57	84.76	0.14
CMT-6	2.50	2.24	154.30	168.82	85.98	0.24
CMT-7	2.35	2.39	161.10	133.50	84.35	0.46
CMT-8	2.63	2.34	149.08 ^b	157.14 ^c	82.39	0.13
HDX ^a	2.40	2.20	136.99	143.96	92.63	0.11

^aDistances for MMP-9-reverse hydroxamate (HDX) complex are taken from Rowsell et al.²¹ ^bThe angle for O12–Zn–N1. ^cThe angle for O12–Zn–N2.

to the value for MMP-2 complexed with the hydroxamate inhibitor (Zn–O = 2.4 Å),²¹ indicating the coordination of the CMT-*n* ligand with the zinc ion. The CMT-1, -2, -4, -6, -7, and -8 act as bidentate ligands suggesting a coordination number of five for Zn ion. For these complexes, we calculated the degree of trigonality (τ) of the zinc metal center. This quantity is computed as in eq 5, where β and α are the largest angles in the metal coordination sphere

$$\tau = |\beta - \alpha|/60 \quad (5)$$

For $\tau = 1$, the structure can be viewed as a perfect D_{3h} trigonal bipyramidal, and for $\tau = 0$, the structure is assigned as C_{4v} square pyramidal.⁶⁴

The analysis of the parameter τ (see Table 2) reveals that the degree of trigonality is close to 0 for most complexes, especially CMT-1 and CMT-2 ($\tau = 0.02$ and 0.07 , respectively), indicating that the geometry around the metal center is almost perfectly square pyramidal. The complex with CMT-7 shows a degree of trigonality $\tau = 0.46$, and in this case, the geometry around the metal center is a mixture of square pyramidal and trigonal bipyramidal. At this point, it is interesting to discuss the

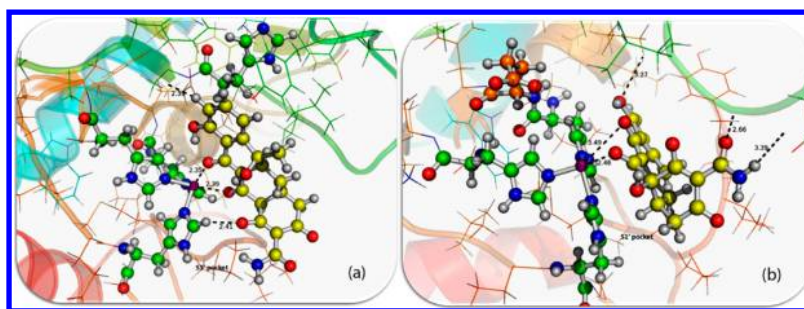


Figure 4. Final MD structures of (a) CMT-7 and (b) CMT-3 complexed with the MMP-2 active site.

influence of the enzyme environment in the geometry adopted by the metal center. In a recent work, the simplest model accounting for only the first coordination shell was investigated considering distinct coordination sites for CMT-*n*.¹¹ On the basis of the values of τ , it was suggested that the geometry of the metal center depends on the ligand binding site and not specifically on the CMT considered. For the complexes involving coordination at the O11–O12 site, τ was close to 1.0 and the geometry around the metal was nearly perfectly trigonal bipyramidal. In the present study, employing the entire catalytic domain of MMP-2, the metal coordination sphere was close to a square pyramidal geometry. This behavior suggests that the second or third coordination spheres around the metal zinc center play a role in the metal geometry.

The previous structural analyses for the MMP-2:CMT-*n* complexes make clear the fact that CMT-3 has a different behavior compared to the other analogues regarding the interaction mode with the active site of MMP-2. In fact, experimental results show this analogue as the most potent MMP inhibitor among the CMTs and the conventional antibiotic tetracycline. The dissociation constants were determined for the MMP-2–CMT-3 complex (74 and 148 μM for K_i and K_i' , respectively).⁵² On the basis of these data, it was found that the CMT-3 is the most potent inhibitor; it appears to inhibit MMP-2 in a competitive manner by binding and blocking the active site directly and modifying or altering the active site of MMP-2 indirectly (noncompetitively). Figure 4 shows the complex of CMT-3 and CMT-7 with the MMP-2 active site after the MD simulations. We can see that CMT-3 is embedding within the site and interacting with the Zn ion through the O12 (2.4 Å) oxygen atom. In addition, the upper side of CMT-3 (ring D), which has no binding groups, is found close to the hydrophobic region of the active site in the MMP-2 enzyme, and thus, the complex with CMT-3 is also stabilized by close hydrophobic contacts with the enzyme environment, mainly residues MET219–TYR223. The carbonyl group at the C1 position is involved in a polar contact with GLY162 (3.3 Å), the hydroxyl at C10 in a hydrophobic contact with VAL198 (2.9 Å), and the amide group at C2am also shows a hydrophobic contact with ASP165 (3.4 Å). This type of interaction has been observed in crystal structures for other complexes with the MMP enzyme.⁶⁵ The position occupied by the CMT-3 analogue inside the active site is totally different from those observed in the complexes with the other CMT-*n* analogues studied here. The other complexes present the ligand coordinated directly with the metal center through the O11–O12 oxygen atoms. The CMT-1 and CMT-4 make two hydrogen bonds with the LYS89 and PRO221 side chains; the CMT-6 and CMT-8 are also hydrogen bonded with LYS89. CMT-7 forms a hydrogen bond with ALA162 (2.4 Å), and the

ring D of CMT-7 makes a hydrophobic contact with TYR155 that is close to the structural zinc of MMP-2 (see Figure 4). GLU202 is involved in a hydrogen bond with the HIS179 side chain in the CMT-7 complex; this GLU residue is very important to the catalytic mechanism of MMPs. Thus, in short, joining the experimental information with the present outcomes, it can be suggested that the coordination with catalytic zinc is not the main feature responsible for inhibition of MMPs, with the occupancy of the S1' pocket playing a major role for biological response. This should be true for those compounds having a hydrophobic moiety, which is essential to drive the molecule; otherwise, the coordination to zinc dominates.

Free Energy Calculations. The TI method was applied to calculate the relative free energy of binding between complexes MMP-2:CMT-3 and MMP-2:CMT-8. These calculations involve a virtual transformation of the CMT-3 into the CMT-8 ligand, which implicates a substitution of the H atoms at C5 and C6 by OH and CH₃ groups, respectively. The $\langle \partial V(\lambda) / \partial \lambda \rangle$ values are plotted in Figure S6 (Supporting Information) as a function of λ for all three transformations considered. To check the dependence of the results on the direction of the mutation (hysteresis), the corresponding curves of the reverse mutations are also presented. The free energy for transformation of unbonded CMT-3 into CMT-8 in solution, $\Delta G_{\text{solv}}^{\text{CMT-3} \rightarrow \text{CMT-8}}$ was 100.3 kcal mol^{−1}, and while bound to the protein $\Delta G_{\text{prt}}^{\text{CMT-3} \rightarrow \text{CMT-8}}$ was 103.0 kcal mol^{−1}. Therefore, the difference in the free energy of binding between the CMT-3 and the CMT-8 was 2.7 kcal mol^{−1}. The free energy for the same mutation calculated in the reverse direction in solution $\Delta G_{\text{solv}}^{\text{CMT-8} \rightarrow \text{CMT-3}}$ was −100.9 kcal mol^{−1}, and while bound to the protein $\Delta G_{\text{prt}}^{\text{CMT-8} \rightarrow \text{CMT-3}}$ was −98.8 kcal mol^{−1} and thus $\Delta \Delta G_{\text{bind}}^{\text{CMT-3} \rightarrow \text{CMT-8}}$ was 3.1 kcal mol^{−1}.

We have observed the good convergence and consistency of the TI calculations. In fact, the high contribution to the binding free energy difference stems from electrostatics interactions (first and third transformation), which is consistent with the characteristics of the groups involved in the transformation such as the polar hydroxyl group.

To evaluate the binding affinities of the CMT-*n* compounds with the active site of the MMP-2 in aqueous solution, we have used the MM-PBSA methodology. The internal dielectric constant was set to 4.00 in order to reproduce the TI value. This calibration of the MM-PBSA approach was done only for the CMT-3 → CMT-8 process. With the TI method, the average value obtained for $\Delta \Delta G_{\text{bind}}^{\text{CMT-3} \rightarrow \text{CMT-8}}$ was 2.9 kcal mol^{−1}, and with the MM-PBSA, with the internal dielectric constant equal to 4.00, the corresponding value was 2.6 kcal mol^{−1}.

The MM-PBSA accounts for contributions represented in eq 4. A set of 300 snapshots have been collected along the latest 6 ns MD trajectory. Table 3 shows the different contributions

Table 3. MM-PBSA Contributions to the Binding Energy Calculated for the CMT-*n* Molecules with the MMP-2 Enzyme

ligand	energy terms (kcal mol ⁻¹)							standard deviation	
	CMT-1	CMT-2	CMT-3	CMT-4	CMT-6	CMT-7	CMT-8	CMT-7	CMT-8
ΔE_{ele}	−74.1	−73.39	−35.40	−103.62	−95.31	−66.50	−69.97	9.68	20.01
ΔE_{vdW}	−15.04	−21.12	−32.98	−16.17	−11.33	−16.99	−13.54	2.74	2.93
ΔG_{PB}	87.28	89.14	57.67	119.1	100.57	72.55	73.73	8.99	18.67
$\Delta G_{\text{nonpolar}}$	−3.9	−4.74	−4.41	−4.12	−3.17	−3.68	−2.8	0.22	0.2
$\Delta E_{\text{ele}} + \Delta G_{\text{PB}}$	13.18	15.75	22.27	15.48	5.26	6.05	3.76		
ΔG_{bind}	−5.76	−10.1	−15.12	−4.8	−9.24	−14.62	−12.57	2.61	2.58
$\Delta\Delta G_{\text{bind}}^a$	9.36	5.02	0	10.32	5.88	0.5	2.55		

^a $\Delta\Delta G_{\text{bind}}$ was calculated with the most stable complex as reference, i.e., CMT-3.

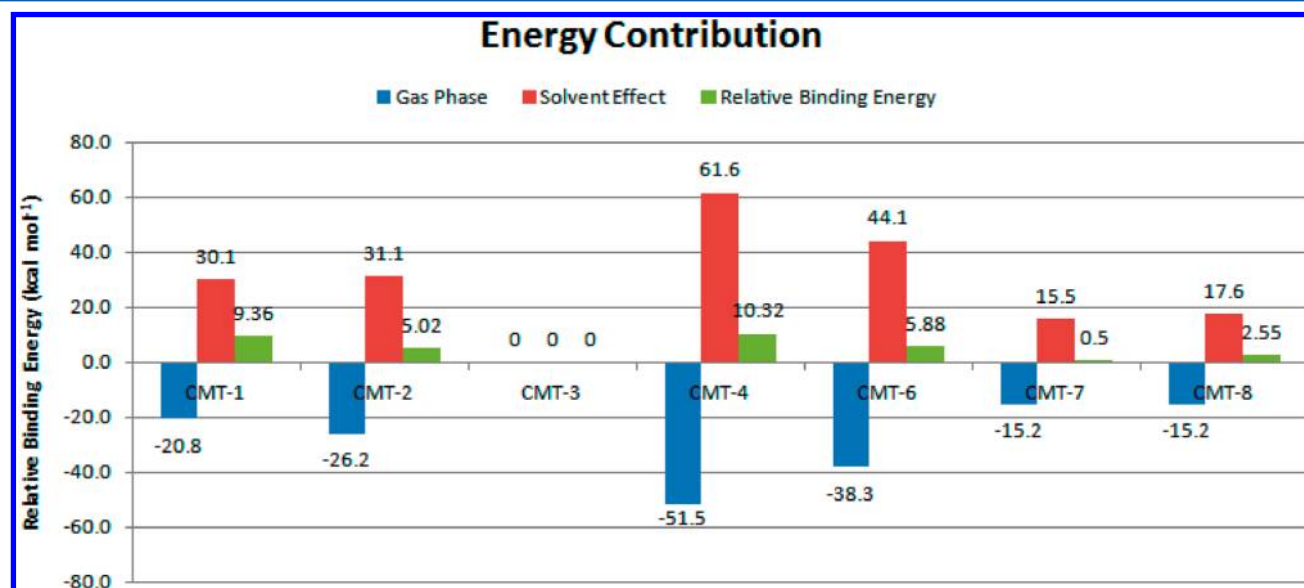


Figure 5. Relative contributions (calculated with the CMT-3 analogue as a reference) to the binding Gibbs free energy for MMP-2 and CMT-*n* obtained with MM-PBSA calculations after calibration with TI.

described in eq 4 for the MMP-2:CMT-*n* complexes including ΔE_{ele} and ΔE_{vdW} from the gas phase and ΔG_{PB} and $\Delta G_{\text{nonpolar}}$ from solution. The standard deviation for the CMT-7 and CMT-8 ligands is also included in Table 3. The gas phase energies favor the binding and the polar solvation free energy disfavors the binding in all complexes. Only the nonpolar contribution from solvent is found slightly negative for complex formation.

As shown in Table 3, the binding energy is dominated by the electrostatic and polar solvation terms, especially in the case of the CMT-4 analogue, which has a Cl group at the C7 position (see Figure 1) and is the least lipophilic among all the CMT analogues. In part, the magnitude of the electrostatic terms is due to the charge of the ligand (−2) in the fully ionized form. The binding energy is the sum of the first four terms in Table 3. We note in Figure 5 that the gas phase energy and the solvent effect are almost of the same size, resulting in a small net binding energy.

From the ΔG_{bind} values, the affinity order for the three more stable complexes is CMT-3 > CMT-7 > CMT-8, whose energy differences are within the standard deviation (~ 3 kcal mol⁻¹). It is worth noting that these complexes show the smaller values of the desolvation penalties ($\Delta G_{\text{SA}} + \Delta G_{\text{PB}}$), mainly CMT-3, which is the most hydrophobic of the CMTs, in contrast to the hydrophilic derivative CMT-4 that showed the largest value for the solvation energy (see Table 3). Thus, in addition to the protein–ligand binding mode discussed previously, the hydro-

phobicity may also be a molecular feature to be considered for structure–activity relationship for CMTs as MMP inhibitors.

Interestingly, in our recent study¹¹ with DFT calculations, using only the first zinc metal coordination shell, the CMT-3 and CMT-8 complexes were found as the most stable in aqueous solution at the DFT level, which is in line with the results found here including the protein backbone.

CONCLUSIONS

In this work, different computational methodologies were applied in order to explore, at the molecular level, the interaction between the CMTs (a new subclass of tetracyclines) and the active site of MMP-2. The mechanism by which CMT-*n*'s inhibit the MMPs has not been completely understood yet. However, besides other weaker interactions, the coordination with the metal ions (Zn) within the enzyme appears to be directly related with the inhibition process. The present study aids to this scenario and might be relevant to design new compounds with improved biological response. The docking methodology was first used to characterize the best position of CMT-*n* inside the active site of MMP-2. The first essays showed that the CMT-*n* occupy the coordination sphere of the zinc ion for most CMT-*n*'s, with one exception found for the CMT-3 analogue, which appears inside the S1' subsite of the enzyme. This is mainly due to the simple structure of CMT-3 that does not have any group at positions C4, C5, C6, and C7.

The structural and energetic findings from the MD simulations provide an explanation for the stability of the complexes formed. The MMP-2–CMT-*n* complexes were stabilized by the interaction of the O11–O12 site of the ligand with the catalytic zinc ion and by hydrogen bonds with the enzyme. The analysis of the coordination sphere of the metal suggests a square pyramidal geometry for the zinc. The CMT-3 analogue, which showed high affinity by MMP-2, is not directly coordinated to zinc but is involved in many van der Waals and hydrophobic contacts with the selective hydrophobic S1' pocket in the MMP-2 enzyme. These results suggest that the coordination with catalytic zinc may not be essential for MMP inhibition, with the occupancy of the S1' pocket an important molecular feature for biological response. Lastly, the binding free energy analysis suggests a higher affinity between the CMT-3 analogue and the MMP-2 active site, followed by CMT-7 and CMT-8, whose energy difference is within 3 kcal mol⁻¹.

■ ASSOCIATED CONTENT

■ Supporting Information

Superimposition of reverse hydroxamate inhibitor docked into MMP-9 (Figure S1). The root-mean-square deviation (RMSD) variation in the MD simulations performed for the MMP-9 (1GKC) (Figure S2); standard deviations for the parametrized bond lengths calculated from the MD simulations (Table S1 and Figure S3) and structure of MMP-9 dynamics simulations using the set of parameters developed in the present work (Figure S4). The distance between the inhibitor and the zinc ion for several X-ray structures, *ab initio* data, and the values obtained using the set of parameters developed in the present work (Figure S5). The values of Zn–N distance for the crystallographic structure (1QIB)¹² and all MMP-2:CMT-*n* complexes (Table S2). $\partial V(\lambda)/\partial \lambda$ (kcal mol⁻¹) as a function of λ for each transformation in direct and reverse directions (Figure S6). The full citations including all authors are provided. This material is available free of charge via the Internet at <http://pubs.acs.org>.

■ AUTHOR INFORMATION

Corresponding Author

*E-mail: sergio.sousa@fc.up.pt (S.F.S.); E-mail: helio.santos@uff.edu.br (H.F.D.S.). Fax: +55 32 3229 3314 (H.F.D.S.). Phone: +55 32 3229 3310 (H.F.D.S.).

Notes

The authors declare no competing financial interest.

■ ACKNOWLEDGMENTS

B.L.M. thanks the Brazilian Agencies CAPES for a doctoral scholarship (Bolsista da Capes – Proc. n°6560-105). M.J.R. and S.F.S. thank the Fundação para a Ciência e Tecnologia (FCT), Portugal, for grants PTDC/QUI-QUI/103118/2008 and PTDC/QUI-QUI/100372/2008. H.F.D.S. and B.L.M. thank the CNPq and FAPEMIG (Proc. No. CEX - APQ-01742-11) for support.

■ REFERENCES

- (1) Zitka, O.; Kukacka, J.; Krizkova, S.; Huska, D.; Adam, V.; Masarik, M.; Prusa, R.; Kizek, R. *Curr. Med. Chem.* **2010**, *17*, 3751–3768.
- (2) Tu, G. G.; Xu, W. F.; Huang, H. M.; Li, S. H. *Curr. Med. Chem.* **2008**, *15*, 1388–1395.
- (3) Acharya, M. R.; Venitz, E.; Figg, W. D.; Sparreboom, A. *Drug Resist. Updates* **2004**, *7*, 195–208.
- (4) Nelson, M.; Hillen, W.; Greenwald, R. A. *Tetracyclines in Biology, Chemistry and Medicine*; Birkhäuser: Boston, MA, 2001; p 336.
- (5) Richards, C.; Pantanowitz, L.; Dezube, B. J. *Pharmacol. Res.* **2011**, *63*, 151–156.
- (6) Griffin, M. O.; Ceballos, G.; Villarreal, F. J. *Pharmacol. Res.* **2011**, *63*, 102–107.
- (7) Seftor, R. E. B.; Seftor, E. A.; De Larco, J. E.; Kleiner, D. E.; Leferson, J.; Stetler-Stevenson, W. G.; McNamara, T. F.; Golub, L. M.; Hendrix, M. J. C. *Clin. Exp. Metastasis* **1998**, *16*, 217–225.
- (8) Chu, Q. S. C.; Forouzesh, B.; Syed, S.; Mita, M.; Schwartz, G.; Cooper, J.; Copper, J.; Curtright, J.; Rowinsky, E. K. *Invest. New Drugs* **2007**, *25*, 359–67.
- (9) Greenwald, R. A. *Pharmacol. Res.* **2011**, *63*, 97–97.
- (10) Greenwald, R. A.; Golub, L. M. *Curr. Med. Chem.* **2001**, *8*, 237–242.
- (11) Marcial, B. L.; Costa, L. A. S.; De Almeida, W. B.; Anconi, C. P. A.; Dos Santos, H. F. *Theor. Chem. Acc.* **2011**, *128*, 377–388.
- (12) Dhanaraj, V.; Williams, M. G.; Ye, Q. Z.; Molina, F.; Johnson, L. L.; Ortwin, D. F.; Pavlovsky, A.; Rubin, J. R.; Skeeane, R. W.; White, A. D.; et al. *Croat. Chem. Acta* **1999**, *72*, 575–591.
- (13) Lee, C. T.; Yang, W. T.; Parr, R. G. *Phys. Rev. B* **1988**, *37*, 785–789.
- (14) Becke, A. D. *Phys. Rev. A* **1988**, *38*, 3098–3100.
- (15) Rassolov, V. A.; Ratner, M. A.; Pople, J. A.; Redfern, P. C.; Curtiss, L. A. *J. Comput. Chem.* **2001**, *22*, 976–984.
- (16) Curtiss, L. A.; Raghavachari, K.; Redfern, P. C.; Rassolov, V.; Pople, J. A. *J. Chem. Phys.* **1998**, *109*, 7764–7776.
- (17) Frisch, M. J.; Trucks, G. W.; Schlegel, H. B.; Scuseria, G. E.; Robb, M. A.; Cheeseman, J. R.; Scalmani, G.; Barone, V.; Mennucci, B.; Petersson, G. A.; et al. *Gaussian 09*; Gaussian, Inc.: Wallingford, CT, 2009.
- (18) Morris, G. M.; Huey, R.; Lindstrom, W.; Sanner, M. F.; Belew, R. K.; Goodsell, D. S.; Olson, A. J. *J. Comput. Chem.* **2009**, *30*, 2785–2791.
- (19) Cerqueira, N. M. F. S. A.; Ribeiro, J.; Fernandes, P. A.; Ramos, M. J. *Int. J. Quantum Chem.* **2011**, *111*, 1208–1212.
- (20) Stote, R. H.; Karplus, M. *Proteins: Struct., Funct., Genet.* **1995**, *23*, 12–31.
- (21) Rowsell, S.; Hawtin, P.; Minshall, C. A.; Jepson, H.; Brockbank, S. M. V.; Barratt, D. G.; Slater, A. M.; McPheat, W. L.; Waterson, D.; Henney, A. M.; et al. *J. Mol. Biol.* **2002**, *319*, 173–181.
- (22) Aqvist, J.; Warshel, A. *Chem. Rev.* **1993**, *93*, 2523–2544.
- (23) Aqvist, J.; Warshel, A. *J. Am. Chem. Soc.* **1990**, *112*, 2860–2868.
- (24) Aqvist, J.; Warshel, A. *J. Mol. Biol.* **1992**, *224*, 7–14.
- (25) Kilstain, A. V.; Warshel, A. *Proteins: Struct., Funct., Bioinf.* **2009**, *77*, 536–550.
- (26) Oelschlaeger, P.; Schmid, R. D.; Pleiss, J. *Biochemistry* **2003**, *42*, 8945–8956.
- (27) Oelschlaeger, P.; Klahn, M.; Beard, W. A.; Wilson, S. H.; Warshel, A. *J. Mol. Biol.* **2007**, *366*, 687–701.
- (28) Hou, T. J.; Zhang, W.; Xu, X. J. *J. Phys. Chem. B* **2001**, *105*, 5304–5315.
- (29) Hu, X.; Balaz, S.; Shelper, W. H. *J. Mol. Graphics Modell.* **2004**, *22*, 293–307.
- (30) Donini, O. A. T.; Kollman, P. A. *J. Med. Chem.* **2000**, *43*, 4180–4188.
- (31) Hou, T. J.; Guo, S. L.; Xu, X. J. *J. Phys. Chem. B* **2002**, *106*, 5527–5535.
- (32) Zhang, W.; Hou, T. J.; Qiao, X. B.; Huai, S.; Xu, X. J. *J. Mol. Model.* **2004**, *10*, 112–120.
- (33) Aqvist, J. *J. Phys. Chem.* **1990**, *94*, 8021–8024.
- (34) Andrae, D.; Haussermann, U.; Dolg, M.; Stoll, H.; Preuss, H. *Theor. Chim. Acta* **1990**, *77*, 123–141.
- (35) Tuccinardi, T.; Martinelli, A.; Nuti, E.; Carelli, P.; Balzano, F.; Uccello-Barretta, G.; Murphy, G.; Rossello, A. *Bioorg. Med. Chem.* **2006**, *14*, 4260–4276.
- (36) Zimmer, M. *Chem. Rev.* **1995**, *95*, 2629–2649.
- (37) Sousa, S. F.; Fernandes, P. A.; Ramos, M. J. *Theor. Chem. Acc.* **2007**, *117*, 171–181.

- (38) Diaz, N.; Suarez, D. *Biochemistry* **2007**, *46*, 8943–8952.
- (39) Cieplak, P.; Cornell, W. D.; Bayly, C.; Kollman, P. A. *J. Comput. Chem.* **1995**, *16*, 1357–1377.
- (40) Bayly, C. I.; Cieplak, P.; Cornell, W. D.; Kollman, P. A. *J. Phys. Chem.* **1993**, *97*, 10269–10280.
- (41) Weiner, S. J.; Kollman, P. A.; Case, D. A.; Singh, U. C.; Ghio, C.; Alagona, G.; Profeta, S.; Weiner, P. *J. Am. Chem. Soc.* **1984**, *106*, 765–784.
- (42) Wang, J. M.; Wolf, R. M.; Caldwell, J. W.; Kollman, P. A.; Case, D. A. *J. Comput. Chem.* **2004**, *25*, 1157–1174.
- (43) Wang, J. M.; Wolf, R. M.; Caldwell, J. W.; Kollman, P. A.; Case, D. A. *J. Comput. Chem.* **2005**, *26*, 114–114.
- (44) Yang, L. J.; Tan, C. H.; Hsieh, M. J.; Wang, J. M.; Duan, Y.; Cieplak, P.; Caldwell, J.; Kollman, P. A.; Luo, R. *J. Phys. Chem. B* **2006**, *110*, 13166–13176.
- (45) Wang, J.; Wang, W.; Kollman, P. A.; Case, D. A. *J. Mol. Graphics Modell.* **2006**, *25*, 247–260.
- (46) Ryckaert, J. P.; Ciccotti, G.; Berendsen, H. J. C. *J. Comput. Phys.* **1977**, *23*, 327–341.
- (47) Steinbrecher, T.; Labahn, A. *Curr. Med. Chem.* **2010**, *17*, 767–785.
- (48) Blondel, A. *J. Comput. Chem.* **2004**, *25*, 985–993.
- (49) Kollman, P. A.; Massova, I.; Reyes, C.; Kuhn, B.; Huo, S. H.; Chong, L.; Lee, M.; Lee, T.; Duan, Y.; Wang, W.; et al. *Acc. Chem. Res.* **2000**, *33*, 889–897.
- (50) Kuhn, B.; Gerber, P.; Schulz-Gasch, T.; Stahl, M. *J. Med. Chem.* **2005**, *48*, 4040–4048.
- (51) Swanson, J. M. J.; Henchman, R. H.; McCammon, J. A. *Biophys. J.* **2004**, *86*, 67–74.
- (52) Lokeshwar, B. L.; Escatel, E.; Zhu, B. Q. *Curr. Med. Chem.* **2001**, *8*, 271–279.
- (53) Simonson, T. *Mol. Phys.* **1993**, *80*, 441–447.
- (54) Steinbrecher, T.; Mobley, D. L.; Case, D. A. *J. Chem. Phys.* **2007**, *127*, No. 214108.
- (55) Perez, M. A. S.; Fernandes, P. A.; Ramos, M. J. *J. Phys. Chem. B* **2010**, *114*, 2525–2532.
- (56) Othersen, O. G.; Beierlein, F.; Lanig, H.; Clark, T. *J. Phys. Chem. B* **2003**, *107*, 13743–13749.
- (57) Dos Santos, H. F.; De Almeida, W. B.; Zerner, M. C. *J. Pharm. Sci.* **1998**, *87*, 190–195.
- (58) Duarte, H. A.; Carvalho, S.; Paniago, E. B.; Simas, A. M. *J. Pharm. Sci.* **1999**, *88*, 111–120.
- (59) Aleksandrov, A.; Simonson, T. *J. Comput. Chem.* **2009**, *30*, 243–255.
- (60) Dos Santos, H. F.; Nascimento, C. S.; Belletato, P.; De Almeida, W. B. *J. Mol. Struct.: THEOCHEM* **2003**, *626*, 305–319.
- (61) Ryan, M. E.; Usman, A.; Ramamurthy, N. S.; Golub, L. M.; Greenwald, R. A. *Curr. Med. Chem.* **2001**, *8*, 305–316.
- (62) Tochowicz, A.; Maskos, K.; Huber, R.; Oltenfreiter, R.; Dive, V.; Yiotakis, A.; Zanda, M.; Bode, W.; Goettig, P. *J. Mol. Biol.* **2007**, *371*, 989–1006.
- (63) Clendeninn, N. J.; Appelt, K. *Matrix Metalloproteinase inhibitors in Cancer Therapy*; Humana Press: Totowa, NJ, 2001; p 262.
- (64) Addison, A. W.; Rao, T. N.; Reedijk, J.; Vanrijn, J.; Verschoor, G. C. *J. Chem. Soc., Dalton Trans.* **1984**, 1349–1356.
- (65) Morales, R.; Perrier, S.; Florent, J. M.; Beltra, J.; Dufour, S.; De Mendez, I.; Manceau, P.; Tertre, A.; Moreau, F.; Compere, D.; et al. *J. Mol. Biol.* **2004**, *341*, 1063–1076.